Novel 3-DOF Reconfigurable Spherical Motion Generator with Unlimited Workspace

Shiu Hang Ip[1] **Chao Chen**[1] **Denny Oetomo**[2]
[1]Department of Mechanical and Aerospace Engineering, Monash University, Australia
Shiu.Ip@eng.monash.edu.au, Chao.Chen@eng.monash.edu.au
[2]Department of Mechanical Engineering, The University of Melbourne, Australia
doetomo@unimelb.edu.au

Abstract

In this paper, an innovative Reconfigurable Spherical Motion Generator (RSMG) is introduced to provide continuous spherical motion and force transmission. The mechanism enables unlimited workspace in 3-DOF spherical motion with rapid, continuous and precise motion capability. The conceptual design, as well as direct and inverse kinematics, are presented here. Singularities of the mechanism are analyzed. An actuation strategy is proposed such that the RSMG is capable of avoiding any types of singularities in order to produce unlimited spherical motion.

1 Introduction

Recent advances in different areas of engineering research have encountered some common challenges, one of which is how to generate unlimited, continuous, and precise spherical motion. For example, a flight simulator needs a motion base with unlimited spherical motion capability, in order to perform faithful simulation [Hosman *et al.*, 2005]. Accordingly, research on the spherical motion generation has been conducted mainly in two different areas: robotics and spherical motors. Under the umbrella of robotics research, spherical motion can be generated through two common topologies: serial (open-chained) mechanisms (e.g. the gimbal mechanisms and the spherical wrist common to industrial robots [Roberts and Repperger, 1994]) and parallel (closed chained) mechanisms, such as the Agile Eye [St Pierre *et al.*, 1996]. Both suffer from the existence of internal and boundary singularities (joint limits) [Oetomo and Ang Jr, 2009] [Gosselin and Wang, 2002], hence none have been successful in producing unlimited and singularity free spherical motion. It should be mentioned that serial topologies generally posses larger workspace, while the parallel counterparts display higher mechanical stiffness.

Under the research area of spherical motors, there are two common methods in producing the desired spherical motion: electromagnetism and piezoelectricity. An electromagnetic spherical motor contains electromagnetic coils in the stator and permanent magnets in the rotor [Chirikjian and Stein, 1999] [Lee and Kwan, 1991] [Yan *et al.*, 2006]. By controlling the magnetic field of the electromagnetic coils, unlimited spherical motion is obtained. One problem of the electromagnetic spherical motor is the large variation of torque transmission due to the complex and changing magnetic field [Yan *et al.*, 2006][Lee *et al.*, 2005]. Piezoelectricity is also utilized to build spherical motors. In [Khoo *et al.*, 2009], three piezoelectric stators actuate the spherical rotor simultaneously, in order to achieve an arbitrary spherical motion of the rotor. However, the serious conflicts among the incompatibly redundant actuation yield low efficiency and precision and also wore the surface of the rotor out quickly. In the approach of [Friend *et al.*, 2004], the force and torque transmission capability and mechanical stiffness are relatively low.

In this paper, a strategy to produce 3DOF spherical motion with unlimited workspace is proposed. The unlimited spherical workspace is achieved by introducing the reconfigurability and redundancy to the kinematic structure of the mechanism. In producing the unlimited workspace, the proposed strategy also inherently overcomes all the internal and boundary singularities of the mechanism. The spherical motion is produced at the rotor through the use of multiple robotic arms, forming closed-chain kinematic topology with the rotor. The other advantages of the resulting design are the high rigidity of the structure and fast response, due to this parallel topology.

The Reconfigurable Spherical Motion Generation (RSMG) is proposed for the application of flight simulator, as shown in Figure 1. A user can seat the rotor of the RSMG andis able to experience unlimited 3-DOF rotational motion and acceleration.

This paper is organised as follows. Section 2 describes

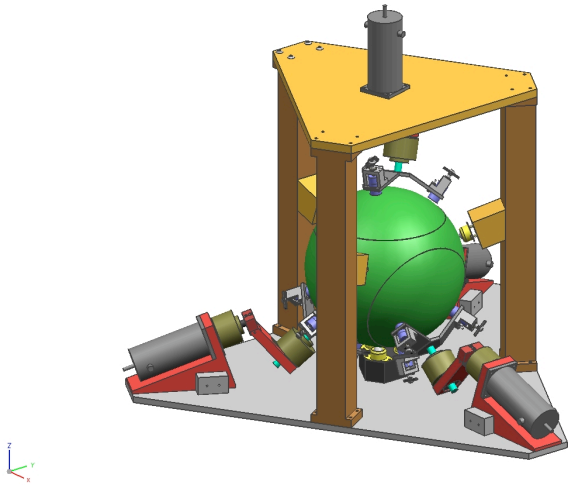

Figure 1: CAD outlook of RSMG

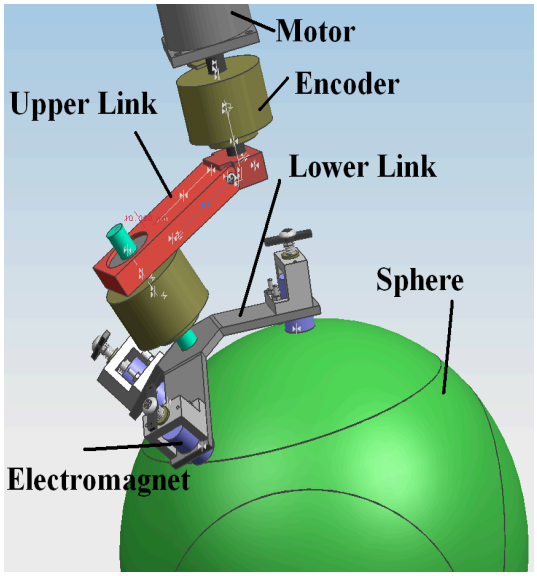

Figure 2: Overview of RSMG with one arm

the concept of the reconfigurable spherical motion generation. Section 3 presents the solutions of direct and inverse kinematics of the mechanism and discusses the singularities of the mechanism. Section 4 provides the operation scheme of the mechanism.

2 Conceptual Design

The conceptual design of the RSMG is shown in Figure 1. The proposed manipulator consists of four motor-actuated robotic arms and one spherical rotor. Each of the robotic arm is a two-link serial mechanism, with the motion of the first link actuated by the motor, while the second is left passive. Encoders are mounted to measure both angular displacements of upper links and lower links. The end effector of each two-link arm is fitted with an electromagnet that attaches to the steel rotor. The rotor is suspended within a ball bearing cage, as shown in Figure 1. Therefore the weight of the rotor is fully supported by the ball bearing cage; the actuated arms are only required to overcome the rotor inertia to generate motion.

Four arms were utilised to produce the 3-DOF spherical motion. The redundant actuation is utilised to overcome singular configurations of the overall resulting parallel mechanism.

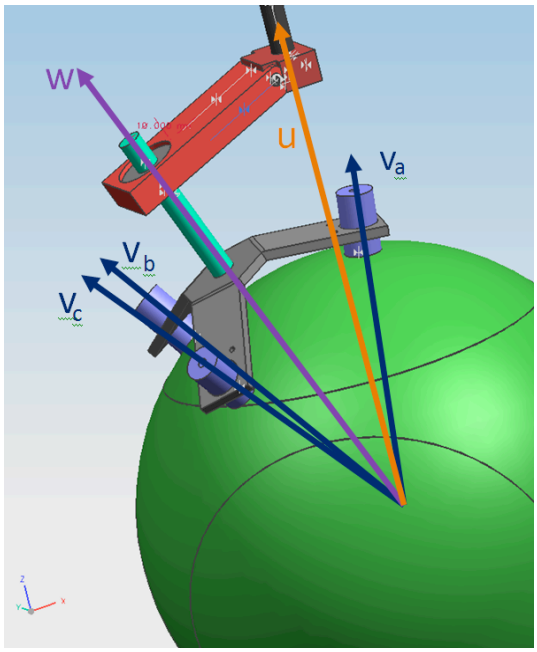

Figure 3: Vectors attached on the arm

2.1 Singularity and Reconfigurability

The mobility of a parallel manipulator is bounded by its singularities. There are two types of singularities in parallel mechanisms: workspace-boundary singularity and workspace-interior singularity [Gosselin and Angeles, 1990].

The main idea of the RSMG is to utilise the reconfigurability of the arms to avoid singularity. When the

mechanism is approaching singularity, it switches to another configuration. Figure 2 shows that each arm consists of an upper link and lower link, with three electromagnets at the end. Only one of the three electromagnets is activated at any instance, creating a two-link mechanism between the associated motor and the spherical rotor. This provides three possible end-effectors for each of the two-link arm, as shown in Figure 2. When the overall mechanism approaches singularity, reconfiguration is carried out by switching the end-effector point to one of the other two alternative attachment points, hence avoiding the singular configuration.

Reconfiguration is carried out by disengaging the magnetic grip of the end-effector to the spherical rotor and activating one of the other two electromagnets on the lower link, thus engaging another point as the end-effector on the spherical rotor. By the reconfigurability of the RSMG, all singular configurations for the parallel spherical mechanism can be avoided. The rotor is therefore driven by four arms simultaneously at any instance, except when reconfiguration is being carried out.

2.2 Reconfiguration Scheme

To achieve the unlimited workspace of the RSMG, it is necessary to establish an intelligent switching algorithm to appropriately reconfigure the mechanism when approaching singularity. In each servo loop, a check is performed to find out if any of the singularities is approaching. This is done by obtaining the explicit expression for the singular configurations and determining when the RSMG has entered a region defined around the exact points of singularities. When this occurs, the mechanism is reconfigured. In this paper, only simple Round-Robin strategy is implemented in determining what configuration to reconfigure the mechanism to. This means, if reconfiguration is to be carried out on arm i, then the electromagnets are simply switched from the current active electromagnet to the next, out of the 3 electromagnets attaching the arm to the rotor.

The workspace-boundary singularities, as identified in [Gosselin and Angeles, 1990], are associated with a specific arm forming the closed-chain configuration. Hence, it is possible to identify exactly which of the four two-link arms is approaching this type of singular configuration. Reconfiguration can therefore be performed on the specific arm to avoid the singular configuration.

The interior singularities are caused by the coupling between the locations of the end-effectors of the arms on the rotor, hence it is not isolated on a specific arm. Another criterion is required to identify which arm needs to be reconfigured, as these singularities are the results of the kinematic interaction between the four arms.

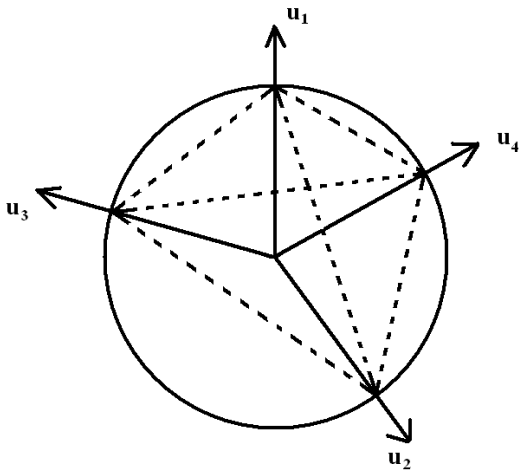

Figure 4: Virtual Tetrahedron

3 Kinematic and Singularity Analysis

Vector u_i is defined as the rotational axis of the upper link of each arm i, where $i = 1, 2, 3, 4$. It should be noted that all four vectors u_i intersect at the centre of the spherical rotor. The locations of the four motors actuating these arms therefore form a tetrahedron as shown in Fig. 4. The three electromagnets acting as the end-effector of each arm i are labelled as EM_a, EM_b, and EM_c. Three vectors V_a, V_b, and V_c are defined from the centre of the spherical rotor to each of the electromagnet, respectively (see Figure 3).

3.1 Mobility Analysis

There are four arm with special arrangements, so that all the axes of revolute joints intersecting at a single point. Further, each arm yields a spherical motion subgroup [Herve, 1999]. The intersection of the four spherical motion subgroup is still the same motion subgroup. Therefore, the rotor has 3 DOF spherical motion.

3.2 Inverse Kinematics

In inverse kinematics of the RSMG, the angular displacements of the active joints (θ_i) are obtained by the given angular displacements of the rotor. Active joint θ_i is angular displacement of the upper link about the rotational vectors u_i. The orientation of the rotor is given such that the locations of the electromagnets V_a of arm i can be determined.

A stationary frame F is defined and attached on the centre of the rotor (see Figure 6). Vectors ${}^F u_i$, ${}^F v_i$ and ${}^F w_i$ are attached to the fixed frame F, where $i = 1, 2, 3$ and 4. Vector ${}^F u_i$ represents the axis of rotation the upper link of arm i and is constant throughout. Vector ${}^F w_i$ goes through the joints connecting the upper and lower links of arm i, while vector ${}^F v_i$ indicates the spherical displacement of the electromagnet a (EM_a). All three

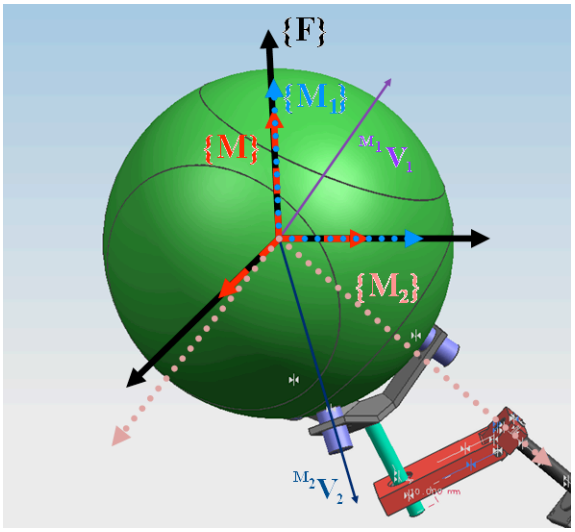

Figure 5: Frame F, M and M_i

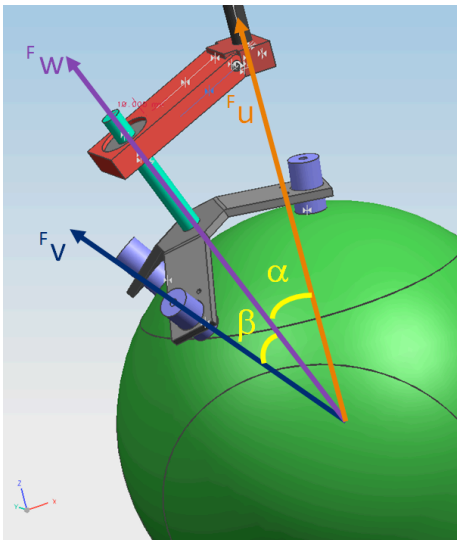

Figure 6: u, v and w in the fixed frame F

vectors ${}^{F}u_i$, ${}^{F}v_i$, and ${}^{F}w_i$ intersect on the centre of the spherical rotor. Angles α is defined between ${}^{F}u_i$ and ${}^{F}w_i$ and β between ${}^{F}w_i$ and ${}^{F}v_i$. Angles α and β represents the angular length of the upper and lower links of the arms, respectively.

Euler angles ϕ_j are defined to represen the Z-Y-X Euler angles, where $j = 1, 2$ and 3. They represent the rotations about the Z, Y and X axes of Frame M. Frame M is defined at the centre of the spherical rotor and moves with the rotor, representing the rotor orientation, such that:

$$\mathbf{{}^{F}_{M}R} = \begin{bmatrix} c_1c_2 & c_1s_2s_3 - s_1c_3 & c_1s_2c_3 + s_1s_3 \\ s_1c_2 & s_1s_2s_3 + c_1c_3 & s_1s_2c_3 - c_1s_3 \\ -s_2 & c_2s_3 & c_2c_3 \end{bmatrix} \quad (1)$$

where $c_j = \cos\phi_j$, $s_j = \sin\phi_j$, $j = 1, 2$ and 3.

${}^{M}v_i$ are the vectors indicating the Ems (EMa only) attached on movable frame M, where $i = 1, 2, 3$ and 4, such that

$$\mathbf{{}^{F}v_i} = \mathbf{{}^{F}_{M}R}\ \mathbf{{}^{M}v_i} \quad (2)$$

Figure 5 shows that fixed frame F is attached to the centre of the rotor. Movable frame M is exactly equal to movable frame M_1. However, for movable frame M_2, M_3 and M_4, it is necessary to map frames in order to obtain ${}^{M}v_2$, ${}^{M}v_3$ and ${}^{M}v_4$. As a result, a set of rotational matrices are necessary to map ${}^{M_i}v_i$ from the movable frame M_i to the movable frame M, such that:

$$\mathbf{{}^{M}v_i} = \mathbf{{}^{M}_{M_i}R}\ \mathbf{{}^{M_i}v_i} \quad (3)$$

${}^{M_i}v_i$ are the vectors indicating the Ems (EMa only) attached on movable frame M_i, where $i = 1, 2, 3$ and 4, such that

$$\mathbf{{}^{M_i}v_i} = \begin{bmatrix} \sin(\alpha+\beta) \\ 0 \\ \cos(\alpha+\beta)) \end{bmatrix} \quad (4)$$

${}^{F}v_i$ are then defined as

$$\mathbf{{}^{F}v_i} = \mathbf{{}^{F}_{M}R}\ \mathbf{{}^{M}_{M_i}R}\ \mathbf{{}^{M_i}v_i} \quad (5)$$

After ${}^{F}v_i$ are obtained, ${}^{F}w_i$ are necessary to be calculated. As shown in Figure 7, there is a set of fixed frames F_i which are employed so that ${}^{F}u_i$ are lay on the z-axes of F_i, such that

$$\mathbf{{}^{F}_{F_i}R} = [\,{}^{F}X_{F_i} \quad {}^{F}Y_{F_i} \quad {}^{F}Z_{F_i}\,] \quad (6)$$

where X, Y and Z are the axes of the frames.

θ_i are the actuator angles which are rotated about ${}^{F}u_i$, where $i = 1, 2, 3$ and 4, representing different actuator angles provided by different motors. ${}^{F_i}_{M_i}R$ is the rotational matrix representing the rotation of the actuator angles, θ_i, such that

$$\mathbf{{}^{F_i}_{M_i}R} = \begin{bmatrix} c_{\theta_i} & -s_{\theta_i} & 0 \\ s_{\theta_i} & c_{\theta_i} & 0 \\ 0 & 0 & 1 \end{bmatrix} \quad (7)$$

where $c_{\theta_i} = \cos\theta_i$, $s_{\theta_i} = \sin\theta_i$ and $i = 1, 2, 3$ and 4.

${}^{M_i}w_i$ are the vectors indicating the joints between upper links and lower links attached on movable frame M_i, where $i = 1, 2, 3$ and 4, such that

$$\mathbf{{}^{M_i}w_i} = \begin{bmatrix} \sin\alpha \\ 0 \\ \cos\alpha \end{bmatrix} \quad (8)$$

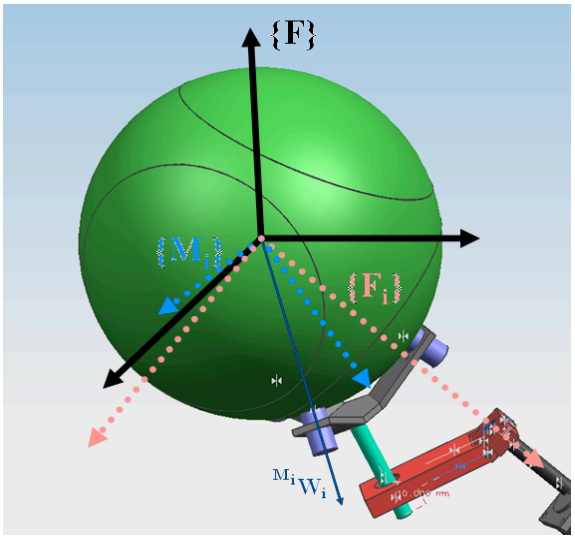

Figure 7: Frame F, F_i and M_i

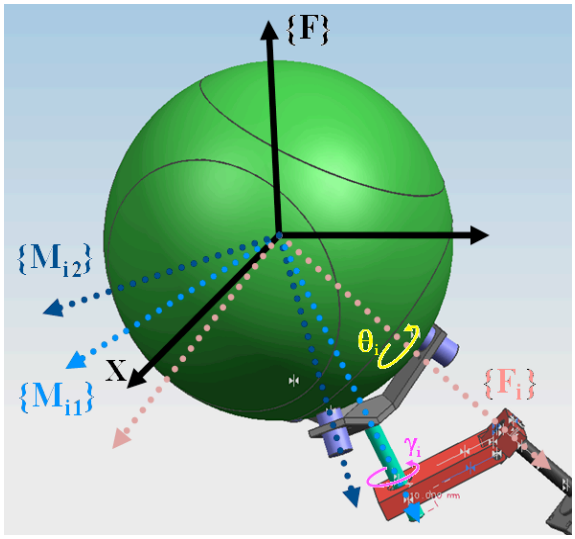

Figure 8: Frame F, F_i, M_{i1} and M_{i2}

${}^{F}w_i$ are then calculated as

$$\mathbf{{}^{F}w_i} = {}^{\mathbf{F}}_{\mathbf{F_i}}\mathbf{R}\ {}^{\mathbf{F_i}}_{\mathbf{M_i}}\mathbf{R}\ \mathbf{{}^{M_i}w_i} \tag{9}$$

There are two constraints in the RSMG, they are

$$\mathbf{{}^{F}w_i} \cdot \mathbf{{}^{F}u_i} = \cos\alpha \tag{10}$$

$$\mathbf{{}^{F}v_i} \cdot \mathbf{{}^{F}w_i} = \cos\beta \tag{11}$$

However, (10) was used in defining ${}^{M_i}w_i$ in (8). Substitute (9) and (5) in (11), we have

$$\mathbf{{}^{F}v_i}^{\mathbf{T}} \begin{bmatrix} {}^{F}X_{F_i} & {}^{F}Y_{F_i} & {}^{F}Z_{F_i} \end{bmatrix} \begin{bmatrix} \cos\theta_i \sin\alpha \\ \sin\theta_i \sin\alpha \\ \cos\alpha \end{bmatrix} = \cos\beta \tag{12}$$

Let

$$\mathbf{g_i}^{\mathbf{T}} = \begin{bmatrix} g_1 & g_2 & g_3 \end{bmatrix} \tag{13}$$

where

$$\mathbf{g_1}^{\mathbf{T}} = \mathbf{{}^{F}v_i}^{\mathbf{T}}\ \mathbf{{}^{F}X_{F_i}} \tag{14}$$

$$\mathbf{g_2}^{\mathbf{T}} = \mathbf{{}^{F}v_i}^{\mathbf{T}}\ \mathbf{{}^{F}Y_{F_i}} \tag{15}$$

$$\mathbf{g_3}^{\mathbf{T}} = \mathbf{{}^{F}v_i}^{\mathbf{T}}\ \mathbf{{}^{F}Z_{F_i}} \tag{16}$$

then, we have

$$\begin{bmatrix} g_1 & g_2 & g_3 \end{bmatrix} \begin{bmatrix} \cos\theta_i \sin\alpha \\ \sin\theta_i \sin\alpha \\ \cos\alpha \end{bmatrix} = \cos\beta \tag{17}$$

rearranging (17), we have

$$g_1 \cos\theta_i g_2 \sin\theta_i = \frac{\cos\beta - g_3\cos\alpha}{\sin\alpha} = g_4 \tag{18}$$

Let

$$\sin\delta = \frac{\mathbf{g_1}}{\sqrt{\mathbf{g_1}^2 + \mathbf{g_2}^2}} \tag{19}$$

$$\cos\delta = \frac{\mathbf{g_2}}{\sqrt{\mathbf{g_1}^2 + \mathbf{g_2}^2}} \tag{20}$$

Finally, θ_i is given by

$$\theta_i = \arcsin(\mathbf{g_4}) - \delta \tag{21}$$

and

$$\theta_i = \pi - \arcsin(\mathbf{g_4}) - \delta \tag{22}$$

where

$$\delta = \arctan(g_1, g_2) \tag{23}$$

3.3 Direct Kinematics

In direct kinematics of the RSMG, the angular displacements of the rotor are obtained by the given angular displacements of the active joints. It is desired to set up encoders to monitor the angles between upper links and lower links, the passive joints (γ_i), which is required in direct kinematics.

Figure 8 shows all the frames, u, v and w required in direct kinematics. As describe in inverse kinematics (6), F_i is a set of frames such that u_i are always lay on the z-axes of F_i. By rotating the X axis, ${}^{F_i}_{M_{i1}}R$ and ${}^{M_{i1}}_{M_{i2}}R$ are defined as in (25 and 26). ${}^{F}_{M_{i2}}R$ are the rotational matrices to map v_i which is defined as follow.

$$\mathbf{{}^{F}_{M_{i2}}R} = {}^{\mathbf{F}}_{\mathbf{F_i}}\mathbf{R}\ {}^{\mathbf{F_i}}_{\mathbf{M_{i1}}}\mathbf{R}\ {}^{\mathbf{M_{i1}}}_{\mathbf{M_{i2}}}\mathbf{R} \tag{24}$$

where

$$\mathbf{{}^{F_i}_{M_{i1}}R} = \begin{bmatrix} c_{\theta_i} & -s_{\theta_i} & 0 \\ s_{\theta_i}c_\alpha & c_{\theta_i}c_\alpha & -s_\alpha \\ s_{\theta_i}s_\alpha & c_{\theta_i}s_\alpha & c_\alpha \end{bmatrix} \tag{25}$$

$$\mathbf{{}^{M_{i1}}_{M_{i2}}R} = \begin{bmatrix} c_{\gamma_i} & -s_{\gamma_i} & 0 \\ s_{\gamma_i}c_\beta & c_{\gamma_i}c_\beta & -s_\beta \\ s_{\gamma_i}s_\beta & c_{\gamma_i}s_\beta & c_\beta \end{bmatrix} \tag{26}$$

and $i = 1, 2, 3$ and 4.

Then ${}^{F}v_i$ is calculated by

$$\mathbf{{}^{F}v_i} = {}^{\mathbf{F}}_{\mathbf{M_{i2}}}\mathbf{R}\ \ {}^{\mathbf{M_{i2}}}\mathbf{v_i} \tag{27}$$

rewrite (5), we have

$$\mathbf{{}^{F}v_i} = {}^{\mathbf{F}}_{\mathbf{M}}\mathbf{R}\ \ {}^{\mathbf{M}}\mathbf{v_i} \tag{28}$$

For ${}^{F}v_i$ and ${}^{M}v_i$, they can be written in matix forms so that K and L are defined, where K is a matrix of all ${}^{M}v_i$ and L is a matrix of all ${}^{F}v_i$ from (27).

$$\mathbf{K} = [\,{}^{\mathbf{M}}\mathbf{v_1} \quad {}^{\mathbf{M}}\mathbf{v_2} \quad {}^{\mathbf{M}}\mathbf{v_3} \quad {}^{\mathbf{M}}\mathbf{v_4}\,] \tag{29}$$

$$\mathbf{L} = [\,{}^{\mathbf{F}}\mathbf{v_1} \quad {}^{\mathbf{F}}\mathbf{v_2} \quad {}^{\mathbf{F}}\mathbf{v_3} \quad {}^{\mathbf{F}}\mathbf{v_4}\,] \tag{30}$$

then, we have

$$\mathbf{L} = {}^{\mathbf{F}}_{\mathbf{M}}\mathbf{R}\ \ \mathbf{K} \tag{31}$$

and finally, we have

$${}^{\mathbf{F}}_{\mathbf{M}}\mathbf{R} = \mathbf{L}\mathbf{K}^{\mathbf{T}}(\mathbf{K}\mathbf{K}^{\mathbf{T}})^{-\mathbf{1}} \tag{32}$$

Finally, the Euler angles can be found by the above equations based on the active joints θ_i and passive joints γ_i .

3.4 Singularity

As mentioned in Section 2, parallel manipulator has singularities. There are two types of singularities, workspace-boundary singularity, workspace-interior singularity and simultaneous singularity [Gosselin and Angeles, 1990]. The kinematic relationship between the active joints and the orientation of the rotor is given by:

$$\mathbf{A}\omega + \mathbf{B}\dot{\theta} = \mathbf{0} \tag{33}$$

where

$$\mathbf{A} = \begin{bmatrix} ({}^{F}w_1 \times^{F} v_1)^T \\ ({}^{F}w_2 \times^{F} v_2)^T \\ ({}^{F}w_3 \times^{F} v_3)^T \\ ({}^{F}w_4 \times^{F} v_4)^T \end{bmatrix} \tag{34}$$

$$\mathbf{B} = \mathbf{diag} \begin{bmatrix} {}^{F}w_1 \times^{F} u_1 \cdot^{F} v_1 \\ {}^{F}w_2 \times^{F} u_2 \cdot^{F} v_2 \\ {}^{F}w_3 \times^{F} u_3 \cdot^{F} v_3 \\ {}^{F}w_4 \times^{F} u_4 \cdot^{F} v_4 \end{bmatrix} \tag{35}$$

3.5 Identify Singularity

As described above, the workspace-interior singularity, type A singularity, occurs when $\det(A) = 0$ and the workspace-boundary singularity, type B singularity, occurs when $\det(B) = 0$.

Workspace-Interior Singularity

Workspace-Interior Singularity based on Matrix A. It is because Matrix A is a 3 by 4 matrix, the rank of A is employed to indicate the workspace-interior singularity. When $Rank(A) = 3$, the motion is singularity-free. When $Rank(A) < 3$, the motion engages singularity.

To avoid type A singularity, it is necessary to avoid $Rank(A) < 3$. Recall (36), we have

$$\mathbf{A} = \begin{bmatrix} ({}^{F}w_1 \times^{F} v_1)^T \\ ({}^{F}w_2 \times^{F} v_2)^T \\ ({}^{F}w_3 \times^{F} v_3)^T \\ ({}^{F}w_4 \times^{F} v_4)^T \end{bmatrix} = \begin{bmatrix} r_1 \\ r_2 \\ r_3 \\ r_4 \end{bmatrix} \tag{36}$$

Assume $r1$ and $r2$ are independent. Then, we make two sub-matrices to determine when it is singular because A is a 4 by 3 matrix.

$$\mathbf{A_1} = \begin{bmatrix} r_1 \\ r_2 \\ r_3 \end{bmatrix} \tag{37}$$

$$\mathbf{A_2} = \begin{bmatrix} r_2 \\ r_3 \\ r_4 \end{bmatrix} = \begin{bmatrix} r_2 \\ \alpha_1 r_1 + \beta_1 r_2 \\ \alpha_2 r_1 + \beta_2 r_2 \end{bmatrix} \tag{38}$$

A is rank-deficient only when A_1 and A_2 are both singular. ie:

$$\mathbf{det(A_1) = 0} \quad \mathbf{and} \quad \mathbf{det(A_2)} = \beta_\mathbf{1}\beta_\mathbf{2} \begin{bmatrix} r_2 \\ r_1 \\ r_1 \end{bmatrix} = \mathbf{0} \tag{39}$$

It is found that if $\mathbf{det(A_1)} = \mathbf{0}$, which means r_1 is dependent on r_2 and r_3. If $\mathbf{det(A_2)} = \mathbf{0}$, which means r_4 is dependent on r_2 and r_3. It implies that A_3 and A_4 are no longer necessary for determining the workspace-interior singularity.

Workspace-Boundary Singularity

To find the workspace-boundary singularity base on Matrix B, we simply set

$$\mathbf{det(B) = 0} \tag{40}$$

it implies

$$|{}^{\mathbf{F}}\mathbf{w_i} \quad {}^{\mathbf{F}}\mathbf{u_i} \quad {}^{\mathbf{F}}\mathbf{v_i}| = \mathbf{0} \tag{41}$$

It means, B is singular when ${}^{F}u_i$, ${}^{F}v_i$ and ${}^{F}w_i$ are coplanar. It means, when γ_i is equal to 0^o or 180^o.

$$\gamma_i = 0^o \quad or \quad 180^o \tag{42}$$

4 Operation Scheme

To avoid singular configurations, an in-build self-reconfiguration scheme is proposed. The scheme predicts the undesired orientations which lead to singular configurations and present a better trajectory between the source and the destiny. There are two main conditions which are set for the self-reconfigurablity. They are based on the singularities which have been discussed in the previous section.

4.1 Operation

In the operation, it is mainly built by a for loop, as the step increases, the data of the whole mechanism is obtained and presented as graph. Finally, an animation is generated based on the obtained data. As it is show in the flow chart, the constants such as α and β are all set as initials. ${}^{F}_{M}R$ and ${}^{F}w_i$ and then calculated. Initially, v_R is calculated as

$$\mathbf{v_R} = {}^{\mathbf{M}}_{\mathbf{M_i}}\mathbf{R}\ {}^{\mathbf{M_i}}\mathbf{v_i} \tag{43}$$

By v_R and ${}^{F}_{M}R$, ${}^{F}v$ is obtained by (5) which is representing the position of EM_a. Using the constraint described in (11), θ_i are calculated. However, there are arbitrary solutions which means an unique solution have to be picked for a continuous animation. After the unique solution is picked, the θ_s are used to calculate w_s. By W_n and W_p, v_b and v_c are found. Then, Γ is calculated base on v_a, v_b, v_c and w_s, where

$$\Gamma = \begin{bmatrix} \gamma_a \\ \gamma_b \\ \gamma_c \end{bmatrix} \tag{44}$$

After the above information has been obtained, switching scheme is then considered. As described above, the switching scheme is base on the singularities of arms. This scheme is called "Round Robin" as it tries to rotate the switching from EM_a, EM_b and EM_c then go back to EM_a. In this proposed scheme, B is considered first then A. The flow chart of "Round Robin" is shown in Figure 10.

4.2 Avoidance of Type B Singularity

It is necessary to switch before the arms have come to singular so that the range of Γ are always between 10^o and 170^o. i.e.

$$10^o < \Gamma < 170^o \tag{45}$$

If the data of the current step meet the requirement, it would go the check with the type A singularity. If not, it would go though them in the order of γ_a, γ_b and then γ_c. If the data couldn't fulfill either of them, it would break out of the loop as shown in Figure 10.

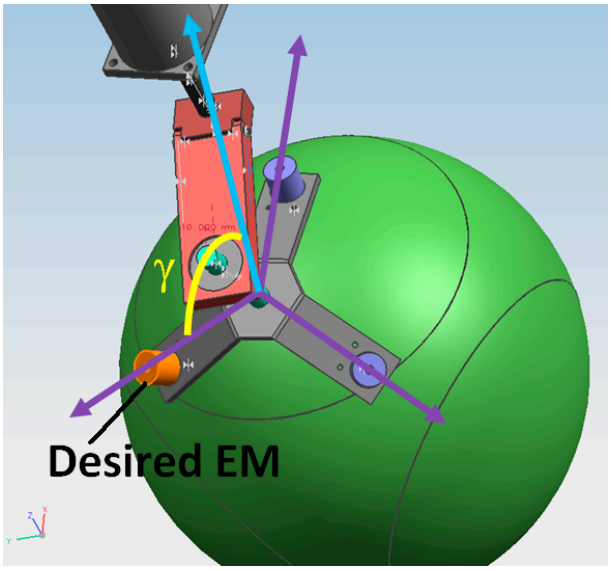

Figure 9: Desired EM and γ

4.3 Avoidance of Type A Singularity

Similar to B, switching before the arms have come to singular is necessary so,

$$\mathbf{-0.01 < |A_1| < 0.01} \quad \textbf{and} \quad \mathbf{-0.01 < |A_2| < 0.01} \tag{46}$$

If the data of the current step meet the requirement, it means the arms are close to singularity surface and switching is required. If not, it would choose the correct vector as the reference vector and present the presentation vector. Finally, the step is added and a new iteration starts.

4.4 Result from Animation of Arm 1

The above operation scheme is applied. The result is animated and shown in Figure 11.

It is found that "Round Robin" allows the lower link to switch in order to avoid singular configurations. As shown in the figure, γ is the angle between the upper link and the lower link with the desired EM, which is attached on the rotor, as shown in 9. When the switching occurs, the angle γ is rearranged and it causes a jumping from roughly 170^o to 10^o.

5 Practical Consideration

In the development of RSMG, there are two practical considerations, the residual magnetism and robust of the electromagnets. The electromagnets are used to attach the rotor firmly, the rotor is then rotated by the arms, not the electromagnets. A test was taken and it showed that the electromagnet is strong enough to hold a steel ball. The residual magnetism will not be a problem,

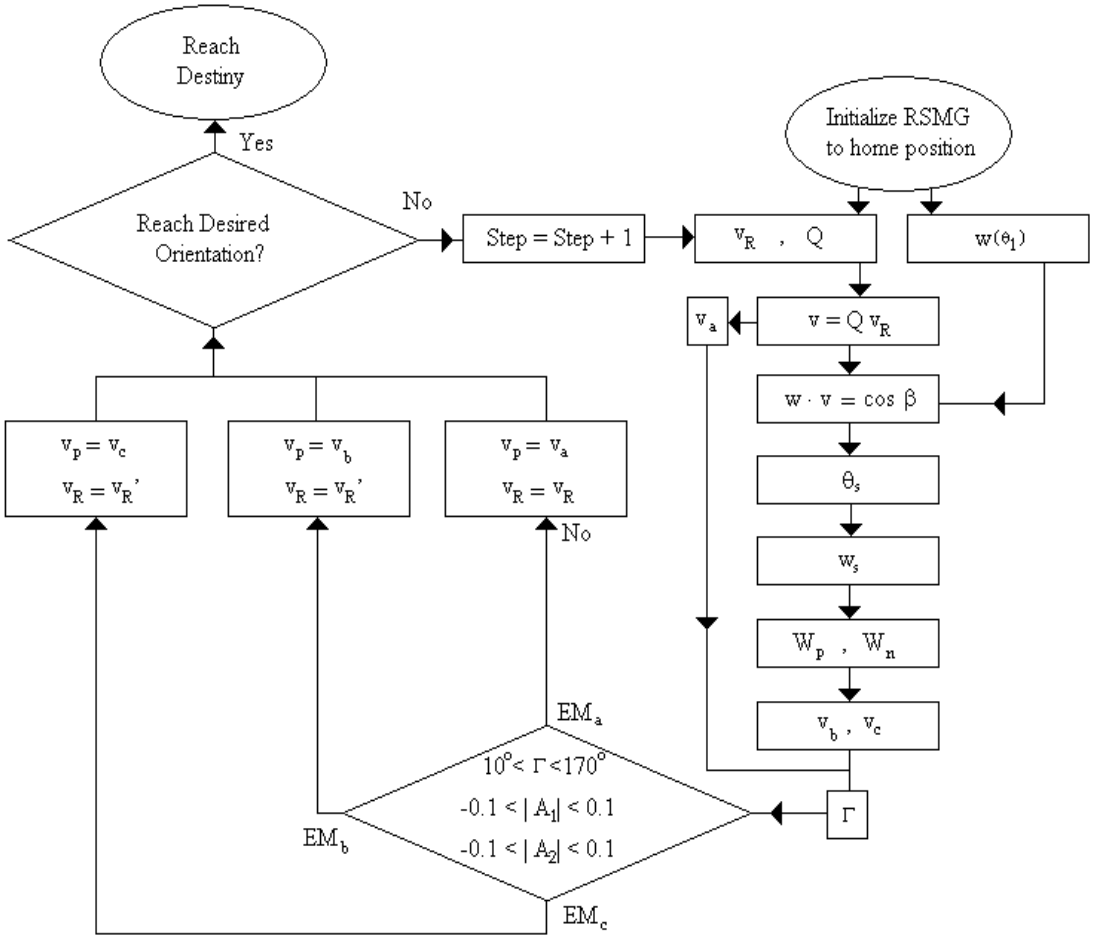

Figure 10: Flow Chart of the Operation Scheme

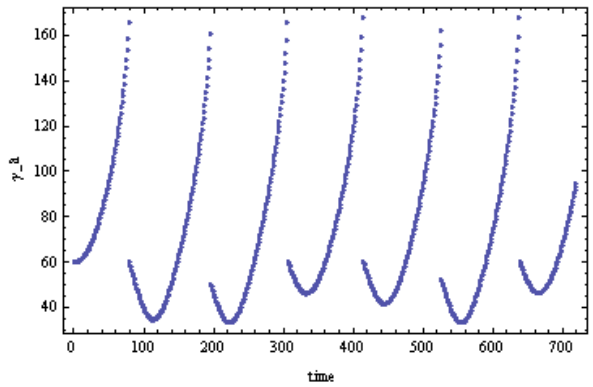

Figure 11: γ against time of Arm 1

because the electromagnets are not attaching to a single point for too long during the reconfiguration. Further, if it occurs, opposite pole of magnet is inducted on the surface of the sphere which enhances the magnetic field.

6 Conclusion

The reconfigurable spherical motion generator (RSMG) is a new mechanism which is able to generate unlimited continuous spherical motion. This mechanism has capability of disengagement and re-engagement. The motion of this redundant device is fully controlled and the undesired configurations are completely avoided. Combining the analysis results of kinematic and singularity and the abilities of disengagement and re-engagement, the operation scheme is developed.

Acknowledgments

The support from ARC Discovery DP0985120 is acknowledged.

References

[Chirikjian and Stein, 1999] G.S. Chirikjian and D. Stein. Kinematic design and commutation of a spherical stepper motor. *IEEE/ASME Transactions on Mechantronics*, 4(4):342–353, 1999.

[Friend *et al.*, 2004] J. Friend, K. Nakamura, and S. Ueha. A piezoelectric micromotor using in-plane shearing of PZT elements. *IEEE/ASME Transactions on Mechatronics*, 9(3):467–473, Sep 2004.

[Gosselin and Angeles, 1990] C. Gosselin and J. Angeles. Singularity analysis of closed-loop kinematic chains. *IEEE Transactions on Robotics and Automation*, 6(3):281–290, June 1990.

[Gosselin and Wang, 2002] C. Gosselin and J. Wang. Singularity loci of a special class of spherical three-degree-of-freedom parallel mechanisms with revolute actuators. *The International Journal of Robotics Research*, 21(7):649–659, July 2002.

[Herve, 1999] J.M. Herve. The lie group of rigid body displacements, a fundamental tool for mechanism design. *Mechanism and Machine Theory*, 34(5):719–730, 1999.

[Hosman *et al.*, 2005] R. Hosman, M. Mayrhofer, M. Wentink, and W. Bles. Design and evaluation of spherical washout algorithm for Desdemona simulator. In *AIAA Modelling and Simulation Technologies Conference*, volume 2, pages 1201–1211, 2005.

[Khoo *et al.*, 2009] T.F. Khoo, D.H. Dang, J. Friend, D. Oetomo, and L. Yeo. Triple degree-of-freedom piezoelectric ultrasonic micromotor via flexural-axial coupled vibration. *IEEE Transactions on Ultrasonics, Ferroelectrics and Frequency Control*, 56(8):1716–1724, Aug 2009.

[Lee and Kwan, 1991] K.M. Lee and C.K. Kwan. Design concept development of a spherical stepper for robotic applications. *IEEE Transactions on Robotics and Automation*, 7(1):175–181, 1991.

[Lee *et al.*, 2005] K.M. Lee, H. Son, and J. Joni. Concept development and design of a spherical wheel motor (SWM). In *the IEEE International Conference on Robotics and Automation*, volume 2005, pages 3652–3657, Barcelona, Spain, April 2005.

[Oetomo and Ang Jr, 2009] D. Oetomo and M.H. Ang Jr. Singularity robust algorithm in serial manipulators. *Robotics and Computer-Integrated Manufacturing*, 25(1):122–134, Feb 2009.

[Roberts and Repperger, 1994] R.G. Roberts and D.W. Repperger. Kinematics of robotics wrists. In *IEEE International Conference on Robotics and Automation*, pages 3337–3341, 1994.

[St Pierre *et al.*, 1996] E. St Pierre, C. Gosselin, and M. Gagne. On the development of the Agile Eye. *IEEE Robotics and Automation Magazine*, 3(4):29–37, 1996.

[Yan *et al.*, 2006] L. Yan, I.M. Chen, G. Yang, and K.M. Lee. Analytical and experimental investigation o nthe magnetic field and torque of a permanent magnet spherical actuator. *IEEE/ASME Transactions on Mechatronics*, 11(4):409–418, Aug 2006.